FINITE ELEMENT AND LOCAL STRAIN APPROACH STRESS-STRAIN PREDICTIONS IN NOTCHED AlCu4.5Mn SPECIMENS

P.S. Ferreira, J. Pinho-da-Cruz and F. Teixeira-Dias

Departamento de Engenharia Mecânica, Universidade de Aveiro
Campus Universitário de Santiago, 3810-193 Aveiro, Portugal

Abstract. Finite element and local strain approach predictions of cyclic stress-strain were investigated for five different types of notched AlCu4.5Mn specimens. Concentration factors for each specimen were determined and compared with those available in literature. Average values and ranges for both elastoplastic stresses and strains were obtained, for several fully-reversed and pulsating nominal traction loading conditions, using non-linear finite element modelling. The obtained results were thoroughly compared and discussed.

1. INTRODUCTION

The existence of structural discontinuities (notches) in mechanical components induces the appearance of localised plastic strains that, combined with cyclic loading, can lead to the initiation of fatigue cracks and, therefore, to structural collapse. Thus, it is imperative to proceed to a precise characterisation of both local stress and strain components. This task is usually performed using non-linear elastoplastic finite element analyses or local strain approach methods, such as Neuber's rule [1] or the Molski-Glinka method [2]. Moreover, commercial finite element programs are generally limited to kinematic and isotropic hardening rules. These rules originate results that are identical for monotonic or proportional loading, but can differ substantially in situations of non-proportional loading or load reversion. In this way, some difficulties may arise when using these programs to model elastoplastic stress-strain states in notches. On this context, the main objectives of this paper are (i) to determine the stress concentration factors of five distinct types of notched specimens using elastic finite element analyses and (ii) to determine, based on finite element and local strain approach methods, mean and range values of local elastoplastic stress and strain for several nominal loadings for some selected notched specimens. In finite element analyses, kinematic and isotropic hardening rules were used. The existence of plane stress and plane stress states at the notch was considered.

2. PREDICTION METHODOLOGIES

Local inelastic stresses and strains can be obtained by two main methodologies: (i) local strain approach, namely by the Neuber's rule or the Molski-Glinka method and (ii) finite element analysis.

2.1 Local strain approach

Cyclic stress-strain curves are generally obtained from uniaxial stress condition tests. They are usually expressed by a Ramberg-Osgood [3] stress-strain expression:

$$\frac{\Delta\varepsilon}{2}=\frac{\Delta\sigma}{2E}+\left(\frac{\Delta\sigma}{2K'}\right)^{\frac{1}{n'}}. \tag{1}$$

Although the cyclic stress-strain curve can describe the stable amplitudes of stress and strain, it cannot generally describe the branches of hysteresis loops that occur in cyclic loading. A material is said to present a Masing-type [4] behaviour if the cyclic stress-strain curve magnification by a factor of two describes the branches of the hysteresis loops. In this situation, the hysteresis loops are described by

$$\Delta\varepsilon=\Delta\sigma+2\left(\frac{\Delta\sigma}{2K'}\right)^{\frac{1}{n'}}. \tag{2}$$

The origin of this curve is located at the compressive tip of the correspondent hysteresis loop.

Neuber's rule and Molsky-Glinka's method relate local and nominal stress ranges, $\Delta\sigma$ and ΔS, to the stress concentration factor Kt, by, respectively, equations

$$K_t^2\frac{\Delta S^2}{4E}=\frac{\Delta\sigma^2}{4E}+\frac{\Delta\sigma}{2}\left(\frac{\Delta\sigma}{2K'}\right)^{\frac{1}{n'}} \tag{3}$$

and

$$K_t^2\frac{\Delta S^2}{4E}=\frac{\Delta\sigma^2}{4E}+\frac{\Delta\sigma}{n'+1}\left(\frac{\Delta\sigma}{2K'}\right)^{\frac{1}{n'}}. \tag{4}$$

The determination of fatigue initiation life can be made using Morrow's modified strain-life equation [5],

$$\frac{\Delta\varepsilon}{2}=\frac{\sigma'_f-\sigma_m}{E}\left(2N_i\right)^b+\varepsilon'_f\left(2N_i\right)^c. \quad (5)$$

Moreover, cyclic and strain-life curves are generally obtained from uniaxial stress tests. However, sometimes a plane strain condition may exist at the notch. This can occur whenever the notch radius is much smaller than the width or thickness of the specimen [6]. In this case, the uniaxial cyclic stress-strain curve must be modified [7,8] to a plane strain Ramberg-Osgood relation between the principal stress/strain,

$$\frac{\Delta\varepsilon_1}{2}=\frac{\Delta\sigma_1}{2E_1}+\left(\frac{\Delta\sigma_1}{2K'_1}\right)^{\frac{1}{n'_1}}, \quad (6)$$

with

$$\frac{\Delta\varepsilon_1}{2}=\frac{\Delta\varepsilon}{2}\frac{\left(1-\mu^2\right)}{\sqrt{1-\mu+\mu^2}}, \quad (7)$$

$$\frac{\Delta\sigma_1}{2}=\frac{\Delta\sigma}{2}\frac{1}{\sqrt{1-\mu+\mu^2}}, \quad (8)$$

$$E_1=\frac{E}{1-\nu^2} \quad (9)$$

and

$$\mu=\frac{\nu+\frac{E\Delta\varepsilon_p}{2\Delta\sigma}}{1+\frac{E\Delta\varepsilon_p}{\Delta\sigma}}. \quad (10)$$

For the same reason, Morrow's modified equation must also be converted to an equivalent one. This strain-life curve in a plane strain condition is given, in terms of the first principal strain amplitude $\Delta\varepsilon_1/2$, by [6]

$$\frac{\Delta\varepsilon_1}{2}=\frac{\frac{\sigma'_f}{\sqrt{1-\mu+\mu^2}}-\sigma_{1m}}{\frac{E}{1-\nu\mu}}\left(2N_i\right)^b+\varepsilon'_f\frac{1-0{,}5\mu}{\sqrt{1-\mu+\mu^2}}\left(2N_i\right)^c, \quad (11)$$

replacing the ranges of stress σ and the plastic strain ε_p by the correspondent first principal ranges, $\Delta\sigma_1/2$ and $\Delta\varepsilon_{1p}/2$, in the generalised Poisson's coefficient μ.

2.2 Finite element and hardening rules

In general, commercial Finite Element codes are limited to the kinematic and isotropic hardening rules using von Mises yield surfaces. These rules predict identical results for uniaxial monotonic tension loading, but severely different results in the case of load reversal. These two hardening rules are illustrated,

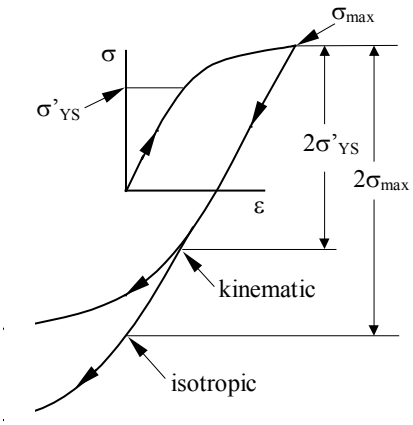

Fig. 1. Kinematic and isotropic behaviours.

for uniaxial loading-unloading behaviour, in figure 1.

As shown, kinematic hardening predicts that yielding in reverse loading occurs with a $2\sigma'_{YS}$ stress change, while isotropic hardening predicts yielding only with a $2\sigma_{max}$ stress change, *i.e.* twice the highest stress level reached prior to unloading. Therefore, kinematic hardening predicts the Bauschinger effect [9] while isotropic hardening does not. This fact can lead to significant discrepancies when modelling cyclic stress-strain behaviour.

A T6 heat-treated AlCu4.5Mn aluminium alloy was considered for research purposes. This alloy, as most aluminium alloys, presents Masing behaviour. It is often used in the aerospacial industry due to its high strength combined with excellent formability. The chemical composition and mechanical properties of this alloy are listed in tables 1 and 2, respectively.

Table 1. Main chemical composition of AlCu4.5Mn alloy (weight. %) [10].

Si	Mg	Mn	Fe	Cu	Zn
0.85	0.50	0.80	1.0	4.5	<0.25

Table 2. Mechanical properties of T6 heat-treated AlCu4.5Mn alloy [10].

Ultimate tensile strength, σ_{UTS} [MPa]	511
Monotonic yield strength, σ_{YS} [MPa]	463
Young's modulus, E [GPa]	69.05
Poisson's coefficient, ν [-]	0.33
Cyclic strain hardening exponent, n' [-]	0.072
Cyclic strength coefficient, K' [MPa]	704

3. FINITE ELEMENT MODELLING

In order to consider the influence of geometrical discontinuities on the local stress and strain values, the behaviour of five distinct notched specimens (*vd.* fig. 2) was numerically modelled using the commercial code Cosmos/M [11]. Specimens 1 and 3 present (*notch radius/minimum diameter*) ratios of 0.125 and 0.1, respectively, both specimens 2 and 4 present a (*notch radius/thickness*) ratio of 2.857 and specimen 5 presents a (*notch radius/thickness*) ratio of 2. The finite element analyses consisted, firstly, in the determination of the stress concentration factors by elastic finite element analyses and, finally, in the computation of inelastic stresses and strains for several monotonic loadings of the specimens using elastoplastic finite element analyses.

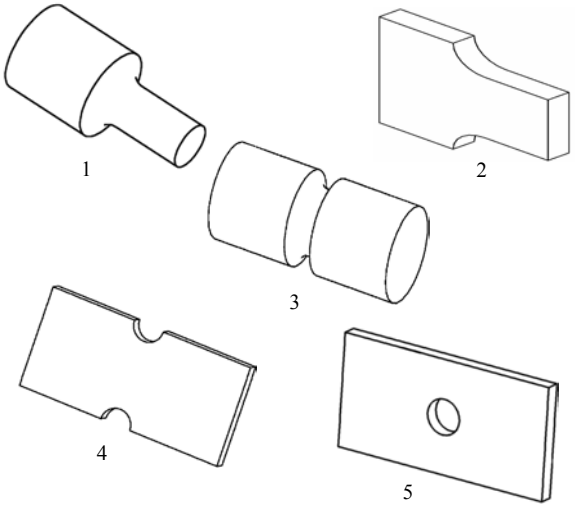

Fig. 2. Types of geometries analysed by finite element.

In order to obtain the stress concentration factors, two-dimensional linear elastic analyses were performed employing 8-node isoparametric quadrilateral elements, for the meshes of specimens 2, 4 and 5, and axisymmetric elements, for meshes of specimens 1 and 3, with full integration. Modelling of specimens was performed considering compatible finite element meshes, which were obtained by performing convergence or mesh refinement studies of the solutions obtained from monotonic axial tension loading analyses. The obtained convergence curves allowed error estimations by the comparison of the last two or three solutions [12]. Since the geometries and loading of the specimens 1 and 2 present only longitudinal symmetry, just half of the specimens was considered in numerical modelling, being their final mesh-type presented in figure 3. Furthermore, since the geometries and loading of the specimens 3, 4 and 5 present both longitudinal and transversal symmetries, only a quarter of the specimens was considered in numerical modelling, being their final mesh-type presented in figure 4.

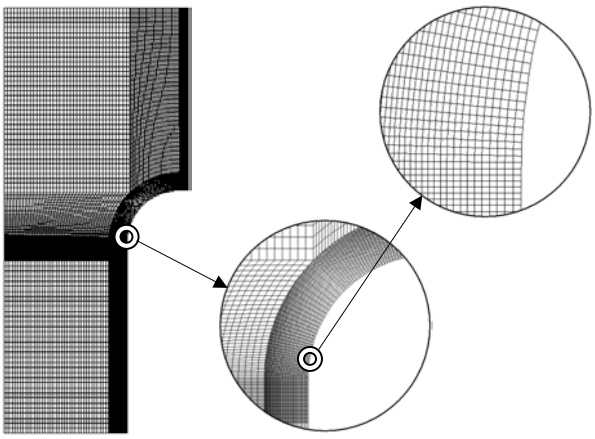

Fig. 3. Mesh-type of specimens 1 and 2.

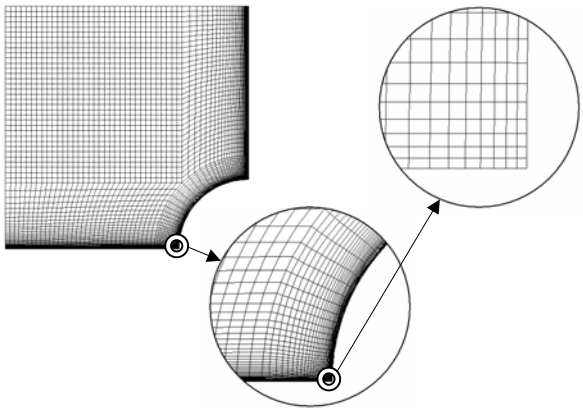

Fig. 4. Mesh-type of specimens 3, 4 and 5.

Due to the localised stress gradients, both meshes were very finely spaced in the vicinity of the respective superficial critical point, as illustrated in figures 3 and 4. The maxima effective longitudinal local stresses σ were measured at the critical surface elements for several nominal axial stresses S, which were defined considering the smallest transversal section area at the notched zone. The value of K_t is the slope of the linear regression of the σ–S relation. Determination of local elastoplastic strains and stresses was performed using a Huber-von Mises plasticity model and kinematic or isotropic hardening rules with a multilinear stress-strain cyclic curve, assuming large plasticity and a large displacement updated lagrangian formulation. A force-controlled loading strategy, as the incremental control technique, and the Newton-Raphson method, as the iterative method, were used to achieve convergence under elastic-plastic conditions. The analyses were performed using, as loading boundary conditions, either pulsating nominal stress loops with 300, 325, 350, 375 and 400 MPa ranges, or fully-reversed nominal stress loops with 600, 650, 700, 750 and 800 MPa ranges. Both plane stress and plane strain analyses were performed.

4. RESULTS AND DISCUSSION

4.1 Stress concentration factors

The stress concentration factors obtained for specimens 1 to 5 are 1.515, 1.765, 1.963, 2.395 and 2.525, respectively. These values differ 0.60, 10.37, -4.08, -7.62 and 2.77 % from those of Peterson [13], respectively. It is worthwhile to note that, due to space limitation in this paper, a non-exhaustive presentation of the main results referring only one type of specimen will be made. In this context, the results obtained for specimen 3, for example, concerning the convergence study and relative variation of the stress concentration factor with the number of degrees of freedom are presented in figures 5 and 6, respectively.

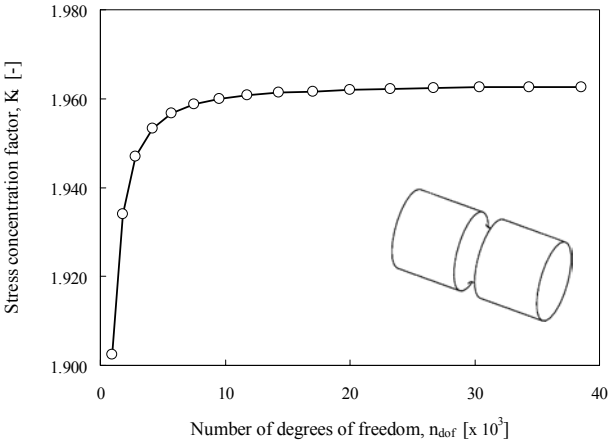

Fig. 5. Convergence study for specimen 3.

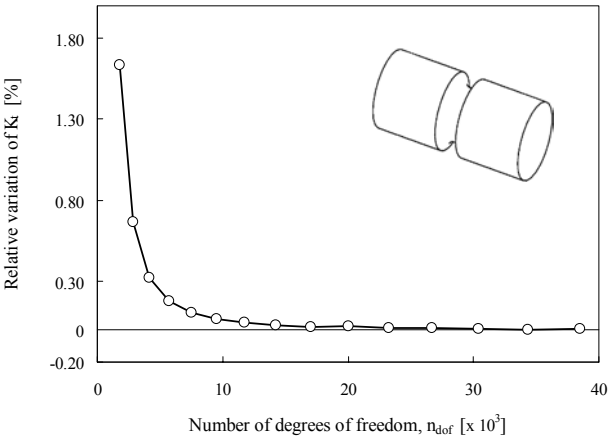

Fig. 6. Relative variation of stress concentration factor with the number of degrees of freedom.

It can be observed that a relative stress concentration factor variation of 5.6×10^{-3} % was obtained for 38521 degrees of freedom. Therefore, the associated final trial solution of 1.963 can be accepted as a converged solution.

A more detailed comparison of the obtained stress concentration factors with those of Peterson [13] was also performed. These results are presented, for specimen 3, in figures 7 and 8 for non-dimensional parameter $\Phi=d/H$ equal to 0.05, 0.1, 0.15, 0.2 and 0.25.

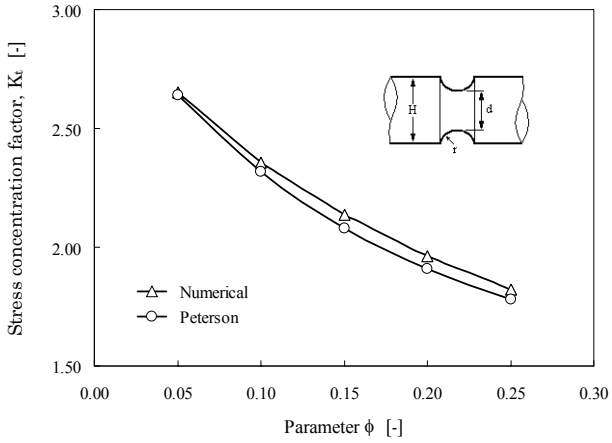

Fig. 7. Comparison of stress concentration factor results with those presented by Peterson [13].

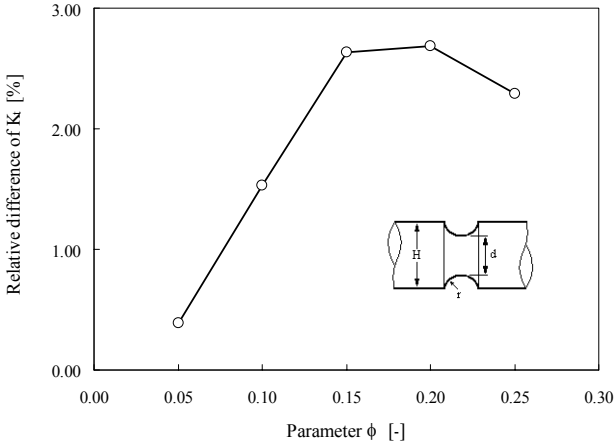

Fig. 8. Relative difference of stress concentration factors.

It can be observed that the numerically obtained values of K_t are, for every value of Φ considered, greater than those of Peterson [13], corresponding to minimum and maximum relative differences of 0.39 and 2.69, respectively. Note that results presented in figures 5 and 6 correspond to a parameter $\Phi=0.2$.

4.2 Stress-strain predictions

Elastoplastic stress-strain prediction results are presented for specimen 5. Figures 9 and 10 illustrate the local elastoplastic finite element stress-strain range and mean predictions, respectively. Plane stress analyses were performed, considering kinematic or isotropic hardening rules, for fully-reversed nominal stress loops with 600, 650, 700, 750 and 800 MPa.

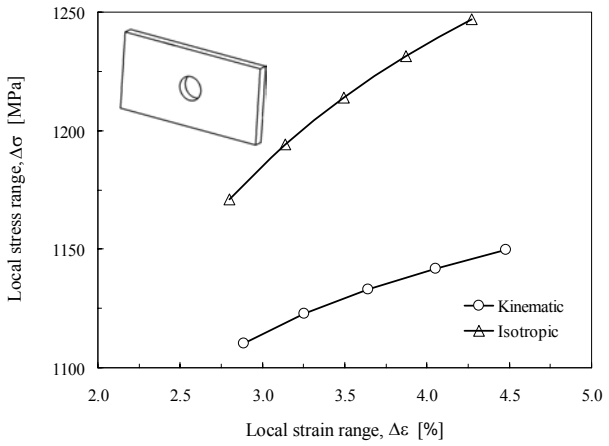

Fig. 9. Kinematic and isotropic local stress *vs.* strain ranges.

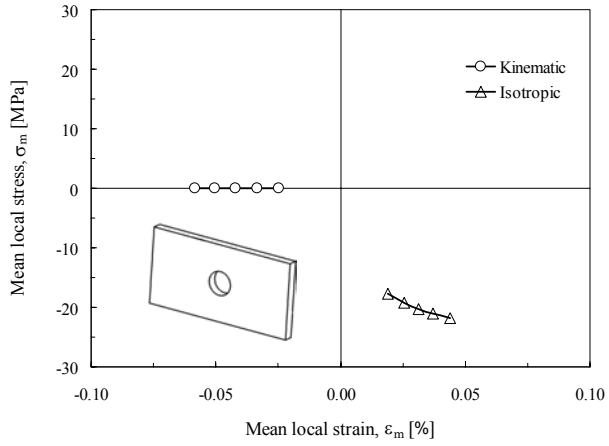

Fig. 10. Kinematic and isotropic local stress *vs.* strain mean values.

From figures 9 and 10, it can be seen that local stress $\Delta\sigma$ predictions obtained when considering isotropic hardening rule are greater than those originated with kinematic hardening rule (*vd.* fig. 9). Moreover, although local strain $\Delta\varepsilon$ predictions are similar for both hardening rule types, mean stress σ_m predictions are null for kinematic hardening and negative for isotropic hardening (*vd.* fig. 10). Therefore, it follows, accordingly to the Morrow's modified strain-life equation (eq. 5), that predictions of fatigue initiation life based on isotropic hardening rule are less conservative than those based on kinematic hardening rule, *i.e.* they predict longer fatigue initiation lives, as illustrated in figure 11. A maximum difference of almost 11 % of number of fatigue initiation cycles is obtained for approximately a 2.8 % local strain range.

Figure 11 illustrates the fact that kinematic and isotropic curves do not overlap. This can be explained by the fact that a negative mean stress leads to a curve translation towards the right, *i.e.* in the direction of greater fatigue initiation lives.

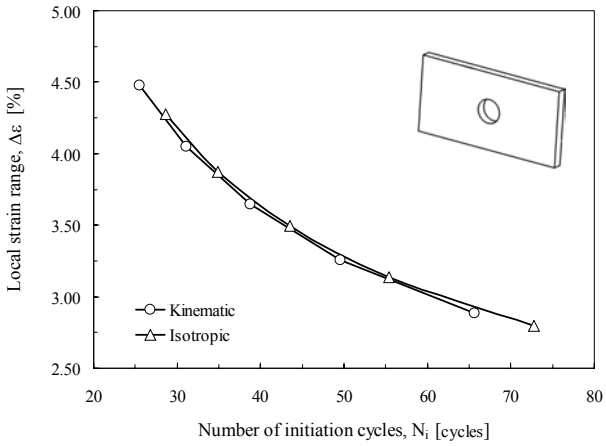

Fig. 11. Kinematic and isotropic fatigue initiation life predictions.

Note that, since the AlCu4.5Mn alloy presents Masing behaviour, it follows that kinematic hardening results may be expected to be more realistic than those of isotropic hardening rule.

Local strain approach and finite element methodologies were carried out, only for kinematic hardening rule, considering nominal fully-reversed stress loops (*vd.* fig. 12) or pulsating stress loops (*vd.* figs. 12 and 13) with 300, 325, 350, 375 and 400 MPa ranges. In these figures the presented acronyms correspond to: FE – finite element, N – Neuber's rule, MG – Molsky-Glinka method, PSTRS – plane stress state, PSTRN – plane strain state and 1D – uniaxial. The local strain approach results obtained for a plane strain state at the notch root were performed using equivalent Young's modulus, E_1, of 77488.5 MPa and equivalent cyclic strain hardening exponent, n'_1, and strength coefficient, K'_1, of 0.0721 and 818.04 MPa, respectively.

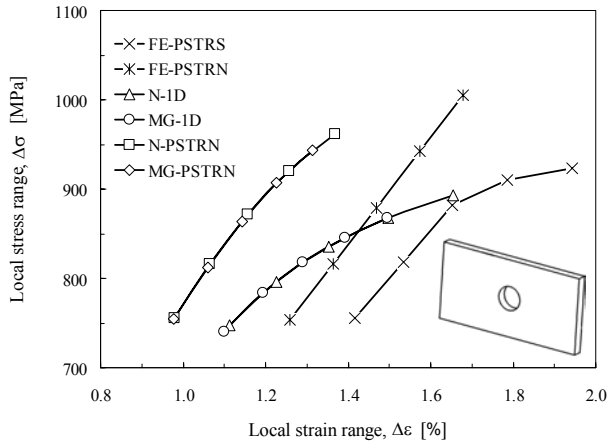

Fig. 12. Local stress *vs.* strain ranges.

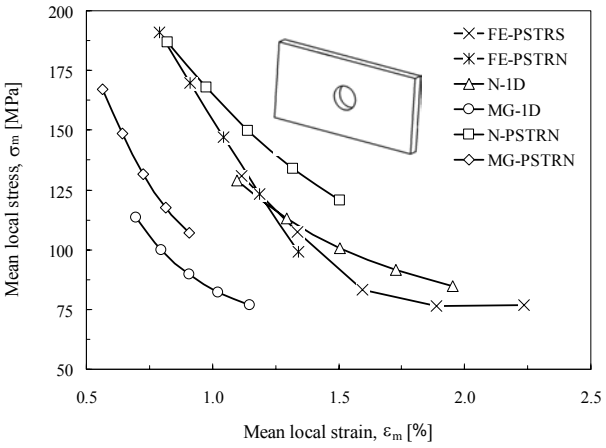

Fig. 13. Mean local stress *vs.* strain values.

The results for specimen 5 illustrate the general tendency of the results obtained for the remainder of specimens. It can be observed that plane stress state finite element predictions correspond to higher $\Delta\varepsilon$ and ε_m and lower σ_m than those of plane strain state finite element, and, for the highest values of nominal stress, to lower $\Delta\sigma$, which evidences the increase of material resistance when subject to a plane strain state. It can also be seen that uniaxial Neuber prediction curves are closer to the finite element predictions than those of Molski-Glinka, although less conservative than the correspondent finite element predictions. Moreover, for both uniaxial or plane strain states the $\Delta\sigma$, σ_m, $\Delta\varepsilon$ and ε_m Neuber's rule predictions are greater than those of Molski-Glinka method (*vd.* figs. 12 and 13), *i.e.* Neuber's rule gives rise to more conservative predictions than Molski-Glinka method, which is in accordance with what was reported by Glinka [14].

5. CONCLUSIONS

In situations of numerical modelling of cyclic loading of AlCu4.5Mn notched specimens when only kinematic or isotropic hardening rules are available, the kinematic rule should be adopted, since it is the most appropriate rule for cyclic loading – it does exhibit a Bauschinger effect. Considerable differences result from the use of either kinematic or isotropic hardening rules. Also, stress-strain predictions obtained by the local strain approach may significantly differ from those of the finite element method. Thus, the selection of a modelling methodology must be criteriously elaborated. Some of the main factors that must be considered in the definition of a methodology concerning the prediction of fatigue initiation life of notched specimens were referred.

6. ACKNOWLEDGEMENTS

The authors J. Pinho-da-Cruz and F. Teixeira-Dias acknowledge financial support given by the FCT – Fundação para a Ciência e a Tecnologia.

7. REFERENCES

[1] Neuber H., "Theory of stress concentration for shear-strained prismatic bodies with arbitrary nonlinear stress-strain law", Journal of Applied Mechanics **28**, 544-550 (1961).

[2] Molski K. and Glinka G., "A method of elastic-plastic stress and strain calculation at a notch root", Materials Science Engineering **50**, 93-100 (1981).

[3] Ramberg W. and Osgood W.R., "Description of stress-strain curves by three parameters, Technical Report **902**, NACA, (1943).

[4] Masing G., "Eigenspannungen und verfestigung beim messing", Proceedings of the 2nd International Congress of Applied Mechanics, pp. 332-335, Zürich, Orell Füssliverlag, 1926.

[5] Morrow J.D., "Cyclic plastic strain energy and fatigue of metals, internal friction, damping and cyclic plasticity", ASTM, STP **378**, 45-87 (1965).

[6] Dowling N.E., "Mechanical behavior of materials: engineering methods for deformation, fracture, and fatigue", Prentice-Hall International Editions, New Jersey, 2nd Ed., 1998.

[7] Hong N. and Shaobo L., "Biaxial stress fatigue life prediction by the local strain method", International Journal of Fatigue **19**(6), 517-522 (1997).

[8] Dowling N.E., Brose W.R. and Wilson W.K., "Notched member fatigue life predictions by the local strain approach", SAE Advances in Engineering **6**, 55-84 (1979).

[9] Bauschinger J., "On the change of the position of elastic limit of iron and steel under cyclic variation of stress", Mitt. Mech.-Tech. Lab. **13**, (1886).

[10] Boller Chr. and Seeger T., "Material data for cyclic loading. Part D: aluminum and titanium alloys", Elsevier, 93-95 (1987).

[11] Cosmos/M - FEA System, Structural Research & Analysis Corporation, LA, USA.

[12] Rizzo A.R., "Estimating errors in FE analyses", Mechanical Engineering, 61-63 (1991).

[13] Pilkey W.D., "Peterson's stress concentration factors", J. Wiley & Sons, New York, 2nd Ed., 1997.

[14] Glinka G., "Relations between the strain energy density distribution and elastic-plastic stress-strain fields near cracks and notches and fatigue life calculation", ASTM, STP **942**, 1022-1047 (1988).